Published in final edited form as:
Neuroimage. 2008 September 1; 42(3): 1047–1055. doi:10.1016/j.neuroimage.2008.05.035.

Frequency Specificity of Functional Connectivity in Brain Networks

Changwei W. Wu[1,2], **Hong Gu**[1], **Hanbing Lu**[1], **Elliot A. Stein**[1], **Jyh-Horng Chen**[2,*], and **Yihong Yang**[1,*]

1*Neuroimaging Research Branch, National Institute on Drug Abuse, NIH, Baltimore, MD, United States*

2*Interdisciplinary MRI/MRS Lab, National Taiwan University, Taipei, Taiwan*

Abstract

Synchronized low-frequency spontaneous fluctuations of the functional MRI (fMRI) signal have been shown to be associated with electroencephalography (EEG) power fluctuations in multiple brain networks within predefined frequency bands. However, it remains unclear whether frequency-specific characteristics exist in the resting-state fMRI signal. In this study, fMRI signals in five functional brain networks (sensorimotor, 'default mode', visual, amygdala, and hippocampus) were decomposed into various frequency bands within a low frequency range (0–0.24 Hz). Results show that the correlations in cortical networks concentrate within ultra-low frequencies (0.01–0.06 Hz) while connections within limbic networks distribute over a wider frequency range (0.01–0.14 Hz), suggesting distinct frequency-specific features in the resting-state fMRI signal within these functional networks. Moreover, the connectivity decay rates along the frequency bands are positively correlated with the physical distances between connected brain regions and seed points. This distance-frequency relationship might be attributed to a larger attenuation of synchrony of brain regions separated with longer distance and/or connected with more synaptic steps.

Introduction

Specific cortical and subcortical regions, where neural activity unfolds, couple to other brain regions forming functional networks associated with cognition and action (Buzsaki and Draguhn, 2004; Varela et al., 2001). Even under a rest condition in the absence of entrained task performance, these brain regions are thought to possess dynamic, synchronized oscillations, upon which the interactions between brain regions or so-called "functional connectivity" can be observed using resting-state functional magnetic resonance imaging (fMRI) techniques (Biswal et al., 1995; Greicius et al., 2003; Hampson et al., 2002; Lowe et al., 1998). Several studies support the assumption that the low-frequency resting-state fMRI fluctuations have a neuronal basis rather than physiological artifacts induced by cardiac pulsations and/or respiration (Cordes et al., 2001; De Luca et al., 2006; Leopold et al., 2003; Lowe et al., 1998), although the exact neurophysiological mechanism of functional connectivity is still under active investigations (Lu et al., 2007; Mantini et al., 2007). Using a

*Please send correspondences to: Yihong Yang, Ph.D., Neuroimaging branch, National Institute on Drug Abuse, NIH, 5500 Nathan Shock Dr., Baltimore, MD 21224, USA, E-mail: YihongYang@intra.nida.nih.gov, Tel: (410)550-1440 ext 334 Fax: (410)550-1441, Or Jyh-Horng Chen, Ph.D., Room 304, Department of Electrical Engineering, National Taiwan University, Sec. 4, No. 1, Roosevelt Rd., Taipei 106, Taiwan, E-mail: jhchen@ntu.edu.tw, Tel: 886-2-2364-8238 Fax:886-2-2364-8238.

temporal cross-correlation method, Biswal et al. first demonstrated functional connectivity within the a frequency range (0–0.08Hz) in sensorimotor networks (Biswal et al., 1995). Subsequently, resting-state fMRI has been widely applied to investigate spontaneous activity in cognitive and sensory networks, as well as pathological alterations in these networks (Greicius et al., 2004; Hampson et al., 2002; Li et al., 2002; Lowe et al., 1998; Lowe et al., 2000).

Electroencephalography (EEG) studies have provided significant evidence of a tight coupling between regional cerebral hemodynamic responses (HDR) and local field potentials (LFP) (Lauritzen and Gold, 2003; Logothetis et al., 2001). Recent studies demonstrated that the HDR corresponding to task stimulation in primate visual cortex correlates specifically with LFP oscillations in the gamma (γ) band (Niessing et al., 2005; Wilke et al., 2006), while the resting-state HDR in the rat somatosensory cortex correlates with LFPs in the lower frequency range, particularly in the δ band (Lu et al., 2007), suggesting spectral differences under distinct physiological conditions. Mantini et al further demonstrated that each functional network corresponds to a specific frequency-specific rhythm (Mantini et al., 2007). These observations imply that functional connectivity may be frequency specific and that frequency characteristics may be distinct for different brain networks. Several previous studies have explored the frequency domain of functional connectivity; some observed frequency relationships on a large scale (Cordes et al., 2001; Salvador et al., 2005; Salvador et al., 2008), while others aimed at topologically reciprocal connections between regions instead of between/within known brain networks (Achard et al., 2006; Salvador et al., 2007).

Our goal, therefore, was to investigate the spectral features of resting-state spontaneous fMRI fluctuations between multiple functional networks with finer frequency intervals. To do so, we assessed the frequency characteristics of BOLD functional connectivity signal in five brain networks (sensorimotor, ‘default mode’, visual, amygdala, and hippocampus). Using multiple band-pass filters with 0.01–0.04 Hz bandwidth, the resting-state fMRI signal was decomposed into 12 frequency bands and analyzed from each of the five networks between 0–0.24 Hz. Both between- and within-network frequency specific disparities were seen in cortical and limbic networks.

Methods

Participants

Twenty healthy participants were included in this study (13 males, 36 ± 9 years-old). They were screened with a questionnaire to ensure that they had no history of neurological illness, psychiatric disorders or past drug use. Present drug use and pregnancy were assessed with urine testing. Informed consent was obtained from all participants prior to the experiments in accordance with the protocol approved by the Institutional Review Board of the National Institute on Drug Abuse.

Data acquisition

Six minutes of resting fMRI data were acquired on a 3.0 T Siemens Allegra scanner (Siemens, Erlangen, Germany) using a single-shot, gradient-recalled echo planar imaging (EPI) sequence (2000 ms repetition time (TR), 27 ms echo time (TE), and 77° flip angle and a head volume coil. Head motion was minimized using individually custom-made foam padding. Thirty-nine axial slices (220 × 220 mm^2 field of view, 64×64 in-plane matrix size, and 4 mm slice thickness), aligned along the anterior commissure - posterior commissure plane allowed for whole brain coverage. Prior to the resting scan, subjects were instructed to rest with their eyes closed, not to think of anything in particular, and not to fall asleep. For spatial normalization and localization, a set of high-resolution T_1-weighted anatomical images (3D-MPRAGE with

256×192×160 matrix size; 1×1×1 mm^3 in-plane resolution; 1000 ms inversion time; TR/TE = 2500/4.38 ms; flip angle = 8°) was acquired on each subject.

Pre-processing

Functional data were processed using the Analysis of Functional Neuroimaging (AFNI) software package (Cox, 1996). Motion correction was performed by volume registering each 3D volume to a base volume. Linear detrending was applied to eliminate signal drift induced by system instability. The images were then converted into Talairach space and linearly resampled to an isotropic resolution (3×3×3 mm^3). Subsequently, spatial smoothing was applied using a Gaussian isotropic kernel (full width at half maximum of 6 mm) to minimize individual variances and enhance the signal-to-noise ratio. The T_1 anatomical image was segmented into gray matter, white matter, and cerebrospinal fluid (CSF) maps using the SPM5 package (Wellcome Institute of Cognitive Neurology, UK).

After these processing procedures, 12 datasets with specific frequency bands (0–0.01, 0.01–0.02, 0.02–0.04, 0.04–0.06, 0.06–0.08, 0.08–0.10, 0.10–0.12, 0.12–0.14, 0.14–0.16, 0.16–0.20, 0.20–0.24 Hz and the typical range of 0–0.1 Hz) were generated using Chebyshev type II low-pass/band-pass filters in MATLAB (MathWorks, Inc., CA). The edges of the bands were constrained within 6 dB decay, while at least 30 dB of attenuation was guaranteed in the stop-bands (pass-band edges ±0.003Hz).

To correct for the potential influence of physiological noise, estimations of cardiac and respiratory information were performed using a temporal independent component analysis (ICA) (Beall and Lowe, 2007). Specifically, twelve components were identified by temporal ICA from our resting-state datasets. Among the spatial patterns of the 12 components, the one with highest spatial correlation with a predefined cardiac source map was considered as the major source of cardiac response. The time courses from the cardiac-correlated map were averaged to generate a cardiac estimator. The same procedure was done to generate a respiratory estimator. These cardiac and respiratory estimators were then used to regress out potential physiological influence in the calculation of correlation coefficients.

Statistical analysis

Spherical seeds (6 mm in diameter) were prescribed for each of the five networks based on standard Talairach coordinates: 1) posterior cingulate cortex (PCC) [3, −54, 24]; 2) primary motor cortex (M1) [36, −28, 53]; 3) primary visual cortex (V1 or BA17) [3, −81, 8]; 4) amygdala (AMG) [23, −5, −15]; and 5) hippocampus (HPC) [30, −24, −9] (Table 1). All spherical seeds were chosen from the right side of the brain. Individual analyses of the 12 frequency bands were carried out on the five networks for every participant using linear regression. The average time series from each spherical seed was taken as the major predictor in the regression model. Other nuisance covariates were also considered (the six motion parameters and the time-series retrieved from the segmented white matter mask).

To compute statistical significance across subjects, the correlation maps from individual subjects were converted to normal-distributed z-score maps accounting for the degrees of freedom (DOF) of each frequency band. The effective DOF was estimated by dividing the number of time points in the time series by a correction factor, which was calculated from the area under the curve of the autocorrelation function (Fox et al., 2005). Group-level analyses were performed in AFNI using mixed-effects ANOVA on the z scores for each frequency band. Corrections for multiple comparisons were executed at the cluster level using Gaussian random field theory (voxel-wise threshold of $p < 10^{-4}$ was applied to the connectivity maps, with a minimum cluster volume threshold of 243 mm^3, yielding an overall false positive $p < 0.05$ as determined by Monte Carlo simulation).

ROI generation

To compare the strength of functional connectivity in the five brain network, a total of twenty regions of interest (ROIs) were generated based on the statistical group results of the typically used low-frequency band (0–0.1Hz) (see Table 1). The ROIs in the sensorimotor network consisted of right M1 (M1-r), left M1 (M1-l), supplementary motor area (SMA), and secondary somatosensory cortex (S2). In the default-mode network, the ROIs included PCC, anterior cingulate cortex (ACC), bilateral inferior parietal cortex (IPC), and bilateral medial temporal gyrus (MTG). BA17, 18 and 19 (roughly corresponding to V1, V2 and V3), and LGN were selected from the AFNI atlas in the visual system. In the amygdala system, right AMG (AMG-r), left AMG (AMG-l), medial prefrontal cortex (MPC), and bilateral insula (ISL) were included, while the right and left hippocampus (HPC-r and HPC-l), MPC and parahippocampal gyrus (PHG) were included as ROIs of the hippocampus seed. Most ROIs in the limbic system, such as AMG-r, AMG-l, HPC-r, HPC-l, and PHG, were chosen based on AFNI atlas structures combined with functional connectivity maps (0–0.1 Hz). The seed voxels embedded in a ROI were excluded in the calculation of average correlation coefficient from the ROI in order to avoid artificial enhancement of the coefficient due to autocorrelation. Lastly, a region of CSF inside the ventricles was manually chosen as a reference region, due to the presumption of its irrelevance with brain functional connectivity.

Results

Fig. 1 and 2 shows the connectivity maps of the cortical and limbic networks, respectively, in each frequency band (the middle row represents the slice location of the seed points). In the cortical networks (visual, ‘default-mode’ and sensorimotor systems; see Fig. 1), the ‘long-distance’ connections to distal brain regions are generally most apparent at the lower frequency ranges (0.01–0.06 Hz); see e.g. the BA17 to LGN area in (a), the PCC to ACC in (b), and ipsilateral to contralateral M1 in (c). At higher frequencies, the long-distance connections become less synchronous, while the ‘short-distance’ connections around the seed points spread over wider frequency ranges. In contrast, the long-distance connections in the two limbic networks (Fig. 2) were strongest at relatively high frequency bands (0–0.14 Hz in amygdala and 0.01–0.10 in hippocampus).

Fig. 3 illustrates the average correlation coefficients between the selected ROIs and corresponding seed points in the five networks over frequency bands. The correlations between seed points and CSF are also shown as references, since the CSF signal is considered to be uncorrelated with signals in brain regions. Regarding the visual and sensorimotor networks (Fig. 3a and 3c), the spectral distributions peak within the 0.01–0.02 Hz range and decrease substantially at higher frequency bands. Similar frequency distributions were observed in the default-mode except that the peak exhibited a slightly wider frequency range (0.01–0.04 Hz). In contrast, the frequency dependency pattern in the two limbic system regions (Fig. 3d–e) either remained relatively constant or decreased slightly and monotonically as a function of frequency. The frequency dependence between cortical and limbic networks can also be demonstrated in F-score maps from the ANOVA ($p < 0.05$, corrected), with frequency as the main factor. As shown in Fig. 4, the locations of the frequency-dependent areas precisely match the spatial patterns of the functional connectivity cortical network maps. However, no significant frequency-dependent area in limbic networks remains around the seeds (green dots in Fig. 4) or around the within-network ROIs, indicating that the resting fMRI signal in limbic networks is independent of the 0–0.24 Hz frequency range. In summary, there was a qualitative frequency specific discrepancy between distinct cortical and subcortical brain networks.

The physical distance between ROIs and seed points also exerted an effect on the functional connectivity networks. Fig. 5a shows the connectivity correlations within the typical frequency range (0–0.1Hz) versus direct seed-ROI Euclidean distances for the five brain networks. The

connectivity strength (as measured by cross correlation) is negatively associated with the physical distance, suggesting that the strength of functional connectivity is attenuated with long-distance propagation. The correlation between the connectivity strength and the distance was −0.74 ($p < 0.002$) in the three cortical systems (black) and −0.63 ($p < 0.05$) in the two limbic systems (red). To further investigate the relationship between the frequency specificity in these networks, a gamma function, $CC(f)=a \cdot (f-b)^c \cdot e^{-(f-b)/d}$, was adopted to fit the frequency-distributed correlations in each ROI. In this equation, the parameters a, b and c were used to describe the offset and rising features of the fitted curve, while the parameter d represented the flatness of the curve in the frequency domain. A low flatness value indicates a high decay rate along frequency, i.e., the connectivity is attributed mainly from low frequency components. Fig. 5b illustrates the fitted flatness versus the physical Euclidean distances for each ROI. The cortical systems have evident negative correlation between flatness and distances (black, R= −0.76, $p < 0.002$), suggesting that the connectivity between seed points and distant ROIs is primarily attributed to ultra-low frequency components. A similar trend was also seen in limbic system networks (Fig. 5b) with higher flatness but a non-significant correlation (red, R= −0.48, $p = 0.14$).

To evaluate the stability of functional connectivity networks across subjects, the absolute coefficients of variation (CV, standard deviation / average correlations) of the 20 participants are presented in Fig. 6 over individual frequency bands for the five brain networks. CVs of low-frequency components (0–0.12 Hz) are approximately two times larger (except for LGN in visual system), while CVs of higher frequency bands (0.12–0.24 Hz) are much larger, than the CVs of the typically used frequency range (0–0.1Hz). This suggests that functional connectivity across individuals is more stable at lower frequency bands than higher frequency bands.

Discussions

In the current study, the frequency response of resting-state functional MRI signals were assessed and compared in five brain networks in twenty normal participants. Results show that both similarities and differences exist in the spontaneous fluctuations spectrograms between and within the examined brain networks. Cross-subject variations in the spectral domain provide evidence that connectivity is generally stable among individuals, particularly at low frequency bands.

The highest connectivity coherence was generally seen in a specific frequency period of the spontaneous fluctuations among these brain networks, especially in the ultra-low frequency range (0.01–0.06 Hz), which agrees well with previous reports (Achard et al., 2006; Salvador et al., 2008). Nevertheless, spectral discrepancies between and within brain networks were also seen. A prominent between-network discrepancy revealed in this study is that the functional connectivity in the three cortical networks is dominated by ultra-low frequencies, whereas that in the two limbic system regions is found in frequency ranges up to 0.14 Hz. Such dissimilarity in the frequency domain implies that either the functional connectivity characteristics in different brain networks can reflect distinct frequency and/or firing pattern, of the underlying electrophysiological signal and/or the signal transduction mechanisms from electrophysiology to hemodynamics might vary in different brain regions. Further studies of simultaneous fMRI and electrophysiological measurements in various brain systems may provide further insight to understand the exact mechanism for this observation. It is also worth mentioning that even though the spectral features of two networks (e.g. visual and sensorimotor systems) were quite similar, their inter-network connectivity seems relatively weak, suggesting an asynchrony between the two fluctuation patterns between these two systems (Fox et al., 2005). Based on these observations, it can be speculated that multiple independent spontaneous oscillations

coexist during the resting state, which may have specific frequency feature characteristics within different brain networks.

A discrepancy of within-network connections in different frequency bands was also revealed. Our data showed that long-distance connections (e.g. contralateral M1) seem to be more frequency specific (peaking at low frequency bands), whereas short-distance connections (e.g. ipsilateral M1) are distributed in a relatively wider frequency range, especially in cortical networks (as shown in Fig. 1 and Fig. 3). We posit that the neurobiological basis of this phenomenon may originate from electrophysiological signals linking the two hemispheres. In support of this conjecture, intracortical LFPs recorded from the lunate sulcus using a 15 electrode array, each at least 2.5 mm apart showed that inter-electrode coherence decreased as frequency and/or distance increased, suggesting that LFPs in lower frequency bands travel a longer distance (Leopold et al., 2003). However, the maximum separation of electrode pairs was 10.6 mm, which is a shorter distance than the within-network connecting regions in the current work. Animal studies recording simultaneous electrophysiological and fMRI signals would be beneficial to validate this hypothesis. Another speculation to the frequency-distance disparity may be attributed to a larger attenuation of synchrony for brain regions separated with longer distance and/or connected by more synaptic steps. Taking the visual systems as an example, synaptic relays follow a direct transmission route (LGN-V1-V2-V3) for simplicity, without taking into account any alternative route from other brain regions. Fig. 3a shows gradual reduction of the connectivity strength from the seed to BA 17, 18 and 19 (corresponding to V1, V2 and V3, and the seed being at BA 17) over all frequency ranges, suggesting that the functional connectivity strength might be dependent on synaptic steps. The weak connection to LGN might be due to low ‘top-down’ modulation during the “closed-eye” state. Similar phenomenon was also observed in the sensorimotor network (Fig. 3c), where the contralateral S1/M1 and SMA (one synaptic step) had stronger connections than S2 (two synaptic steps). Of course, differences in hemodynamics, extent of anatomical divergence and convergence, firing patterns and rates, density of vasculatization and coupling mechanics could also explain our observation. The quantitative dependence of functional connectivity on synaptic steps and physical distance, as well as the associated physiological and hemodynamic mechanisms, may be better revealed using animal models with combined anatomical, electrophysiological and fMRI studies.

Multiple cerebral networks during the resting state have also been consistently identified using data-driven approaches such as independent component analysis (ICA) (Damoiseaux et al., 2006; De Luca et al., 2006), implying that independent physiological mechanisms may co-exist in these brain regions to sustain the network functions at rest. Effort has been made to understand the linkage between the fMRI fluctuations and their possible neuronal basis. Recently Mantini et al. provided preliminary neurobiological evidence using simultaneous BOLD-EEG acquisition in human subjects (Mantini et al., 2007). Their results showed that each brain network is differentially weighted to different rhythms in the EEG power spectrum, which might be consistent with our frequency analysis results. However, due to poor spatial resolution in EEG recordings, it may be premature to compare the EEG frequency response directly to the fMRI response. Furthermore, the signal transduction from electrophysiology to hemodynamics might be nonlinear in terms of frequency response.

Physiological noise, including the cardiac/respiratory-induced signal changes and variations in respiration depth, can reduce the power in functional connectivity analysis (Birn et al., 2006; Lowe et al., 1998; Raj et al., 2001). Cordes et al. suggested that respiratory (0.1–0.5 Hz) and cardiac (0.6–1.2 Hz) fluctuations contribute less than 10% of the connectivity in visual and auditory cortices in humans, using a directly-sampled acquisition and a larger frequency binning compared to the current study (Cordes et al., 2001). Nevertheless, variations in respiration depth are particularly problematic in resting-state fMRI data because it is associated

with the ultra-low frequency range (~0.03 Hz). To minimize this artifact, regressing out the global signal has been suggested to provide comparable results to removal of low-frequency respiratory fluctuations (Birn et al., 2006). In this study, the average signal retrieved from white matter was used as a nuisance covariate regressor for each subject, which preserves the involvement of cortical signal and retains the global variation. We have also used a newly developed method to estimate the cardiac and respiratory related time courses by temporal ICA (Beall and Lowe, 2007), and then corrected for the potential influence of physiological noise.

Conclusion

We have examined the spectral response of the resting-state fMRI signal in multiple functional networks of the human brain. The connections in three different cortical networks concentrate within the ultra-low frequencies (0.01–0.06 Hz) while the connections in two limbic networks distribute over a wider frequency range (0.01–0.14 Hz), suggesting distinct frequency-specific features in the resting state fMRI signal across these functional networks. Discrepancies between these networks suggest that distinct physiological mechanisms, perhaps related to differences in 'spontaneous' neuronal firing rates or patterns, may co-exist in these brain regions to sustain the network functions at rest. It has also been shown that the spectral flatness along the frequency range is negatively correlated with the physical distance from brain 'target' regions to the seed. We suggest that connectivity strength may be related to the number of synaptic steps or distance between brain regions. These frequency-specific and anatomic-dependent properties may help interpret the sensitivity and specificity of the resting-state fMRI signal, and should be taken into account in analyzing and interpreting resting-state fMRI data.

Acknowledgements

This work was supported by the Intramural Research Program of the National Institute on Drug Abuse (NIDA), National Institute of Health (NIH). We would like to thank Mark Lowe and Erik Beall of the Cleveland Clinic Foundation for providing software to correct for physiological noise, Thomas Ross of the National Institute on Drug Abuse and Michael Fox of Washington University for helpful discussions on data analysis.

Reference List

Achard S, Salvador R, Whitcher B, Suckling J, Bullmore E. A resilient, low-frequency, small-world human brain functional network with highly connected association cortical hubs. J.Neurosci 2006;26:63–72. [PubMed: 16399673]

Beall EB, Lowe MJ. Isolating physiologic noise sources with independently determined spatial measures. Neuroimage 2007;37:1286–1300. [PubMed: 17689982]

Birn RM, Diamond JB, Smith MA, Bandettini PA. Separating respiratory-variation-related fluctuations from neuronal-activity-related fluctuations in fMRI. Neuroimage 2006;31:1536–1548. [PubMed: 16632379]

Biswal B, Yetkin FZ, Haughton VM, Hyde JS. Functional connectivity in the motor cortex of resting human brain using echo-planar MRI. Magn Reson.Med 1995;34:537–541. [PubMed: 8524021]

Buzsaki G, Draguhn A. Neuronal oscillations in cortical networks. Science 2004;304:1926–1929. [PubMed: 15218136]

Cordes D, Haughton VM, Arfanakis K, Carew JD, Turski PA, Moritz CH, Quigley MA, Meyerand ME. Frequencies contributing to functional connectivity in the cerebral cortex in "resting-state" data. AJNR Am.J.Neuroradiol 2001;22:1326–1333. [PubMed: 11498421]

Cox RW. AFNI: software for analysis and visualization of functional magnetic resonance neuroimages. Comput.Biomed.Res 1996;29:162–173. [PubMed: 8812068]

Damoiseaux JS, Rombouts SA, Barkhof F, Scheltens P, Stam CJ, Smith SM, Beckmann CF. Consistent resting-state networks across healthy subjects. Proc.Natl.Acad.Sci.U.S.A 2006;103:13848–13853. [PubMed: 16945915]

De Luca M, Beckmann CF, De SN, Matthews PM, Smith SM. fMRI resting state networks define distinct modes of long-distance interactions in the human brain. Neuroimage 2006;29:1359–1367. [PubMed: 16260155]

Fox MD, Snyder AZ, Vincent JL, Corbetta M, Van E, Raichle ME. The human brain is intrinsically organized into dynamic, anticorrelated functional networks. Proc.Natl.Acad.Sci.U.S.A 2005;102:9673–9678. [PubMed: 15976020]

Greicius MD, Krasnow B, Reiss AL, Menon V. Functional connectivity in the resting brain: a network analysis of the default mode hypothesis. Proc.Natl.Acad.Sci.U.S.A 2003;100:253–258. [PubMed: 12506194]

Greicius MD, Srivastava G, Reiss AL, Menon V. Default-mode network activity distinguishes Alzheimer's disease from healthy aging: evidence from functional MRI. Proc.Natl.Acad.Sci.U.S.A 2004;101:4637–4642. [PubMed: 15070770]

Hampson M, Peterson BS, Skudlarski P, Gatenby JC, Gore JC. Detection of functional connectivity using temporal correlations in MR images. Hum.Brain Mapp 2002;15:247–262. [PubMed: 11835612]

Lauritzen M, Gold L. Brain function and neurophysiological correlates of signals used in functional neuroimaging. J.Neurosci 2003;23:3972–3980. [PubMed: 12764081]

Leopold DA, Murayama Y, Logothetis NK. Very slow activity fluctuations in monkey visual cortex: implications for functional brain imaging. Cereb.Cortex 2003;13:422–433. [PubMed: 12631571]

Li SJ, Li Z, Wu G, Zhang MJ, Franczak M, Antuono PG. Alzheimer Disease: evaluation of a functional MR imaging index as a marker. Radiology 2002;225:253–259. [PubMed: 12355013]

Logothetis NK, Pauls J, Augath M, Trinath T, Oeltermann A. Neurophysiological investigation of the basis of the fMRI signal. Nature 2001;412:150–157. [PubMed: 11449264]

Lowe MJ, Dzemidzic M, Lurito JT, Mathews VP, Phillips MD. Correlations in low-frequency BOLD fluctuations reflect cortico-cortical connections. Neuroimage 2000;12:582–587. [PubMed: 11034865]

Lowe MJ, Mock BJ, Sorenson JA. Functional connectivity in single and multislice echoplanar imaging using resting-state fluctuations. Neuroimage 1998;7:119–132. [PubMed: 9558644]

Lu H, Zuo Y, Gu H, Waltz JA, Zhan W, Scholl CA, Rea W, Yang Y, Stein EA. Synchronized delta oscillations correlate with the resting-state functional MRI signal. Proc.Natl.Acad.Sci.U.S.A 2007;104:18265–18269. [PubMed: 17991778]

Mantini D, Perrucci MG, Del GC, Romani GL, Corbetta M. Electrophysiological signatures of resting state networks in the human brain. Proc.Natl.Acad.Sci.U.S.A 2007;104:13170–13175. [PubMed: 17670949]

Niessing J, Ebisch B, Schmidt KE, Niessing M, Singer W, Galuske RA. Hemodynamic signals correlate tightly with synchronized gamma oscillations. Science 2005;309:948–951. [PubMed: 16081740]

Raj D, Anderson AW, Gore JC. Respiratory effects in human functional magnetic resonance imaging due to bulk susceptibility changes. Phys.Med.Biol 2001;46:3331–3340. [PubMed: 11768509]

Salvador R, Martinez A, Pomarol-Clotet E, Gomar J, Vila F, Sarro S, Capdevila A, Bullmore E. A simple view of the brain through a frequency-specific functional connectivity measure. Neuroimage 2008;39:279–289. [PubMed: 17919927]

Salvador R, Martinez A, Pomarol-Clotet E, Sarro S, Suckling J, Bullmore E. Frequency based mutual information measures between clusters of brain regions in functional magnetic resonance imaging. Neuroimage 2007;35:83–88. [PubMed: 17240167]

Salvador R, Suckling J, Schwarzbauer C, Bullmore E. Undirected graphs of frequency-dependent functional connectivity in whole brain networks. Philos.Trans.R.Soc.Lond B Biol.Sci 2005;360:937–946. [PubMed: 16087438]

Varela F, Lachaux JP, Rodriguez E, Martinerie J. The brainweb: phase synchronization and large-scale integration. Nat.Rev.Neurosci 2001;2:229–239. [PubMed: 11283746]

Wilke M, Logothetis NK, Leopold DA. Local field potential reflects perceptual suppression in monkey visual cortex. Proc.Natl.Acad.Sci.U.S.A 2006;103:17507–17512. [PubMed: 17088545]

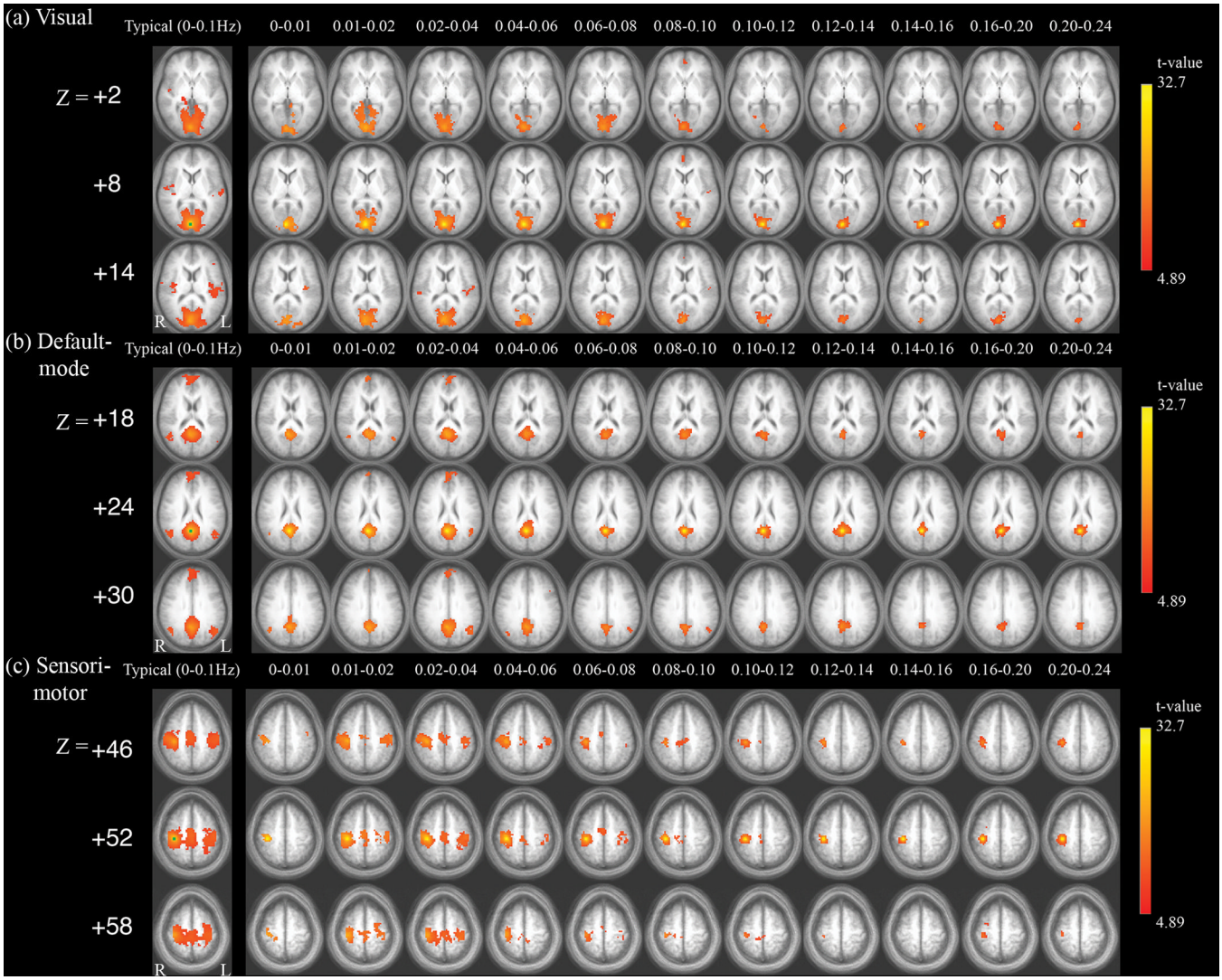

Figure 1.

Frequency-specific functional connectivity maps ($p < 0.05$, corrected) of the three cortical networks: (a) visual system, (b) default mode, and (c) sensorimotor system. The left-most columns denote the functional connectivity maps within the typical frequency range (0–0.1Hz) and the green dots denote the position of the seed points.

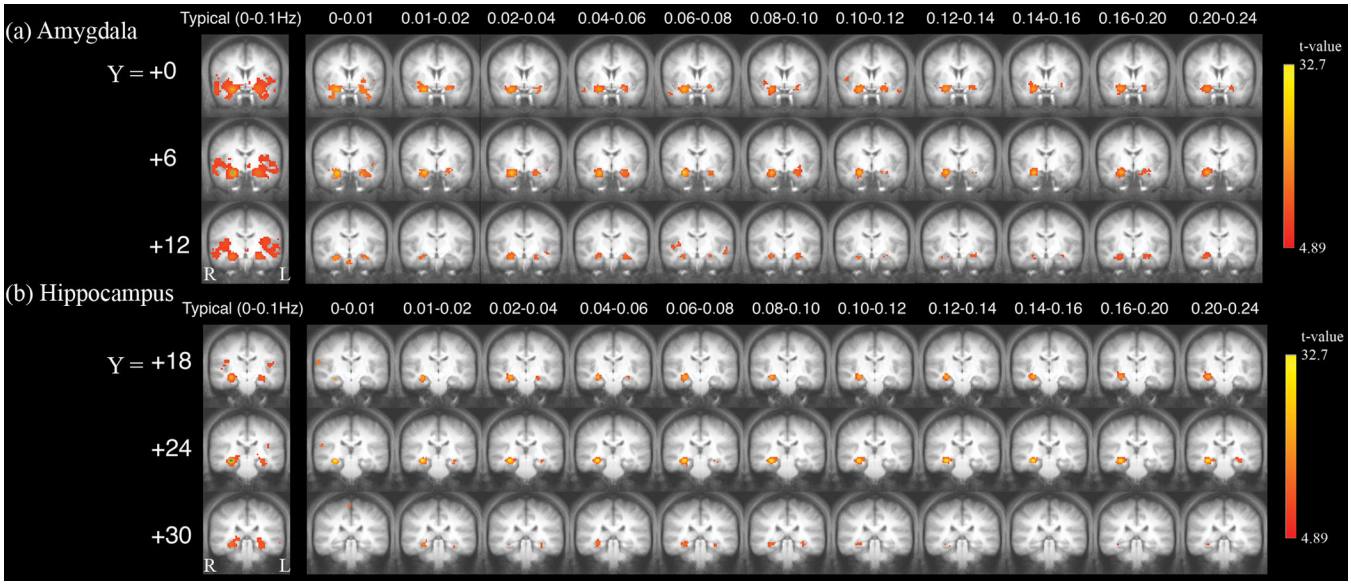

Figure 2.

Frequency-specific functional connectivity maps ($p < 0.05$, corrected) of the two limbic networks: (a) amygdala and (b) hippocampus. The left-most columns denote the functional connectivity maps within the typical frequency range (0–0.1Hz) and the green dots denote the position of the seed points.

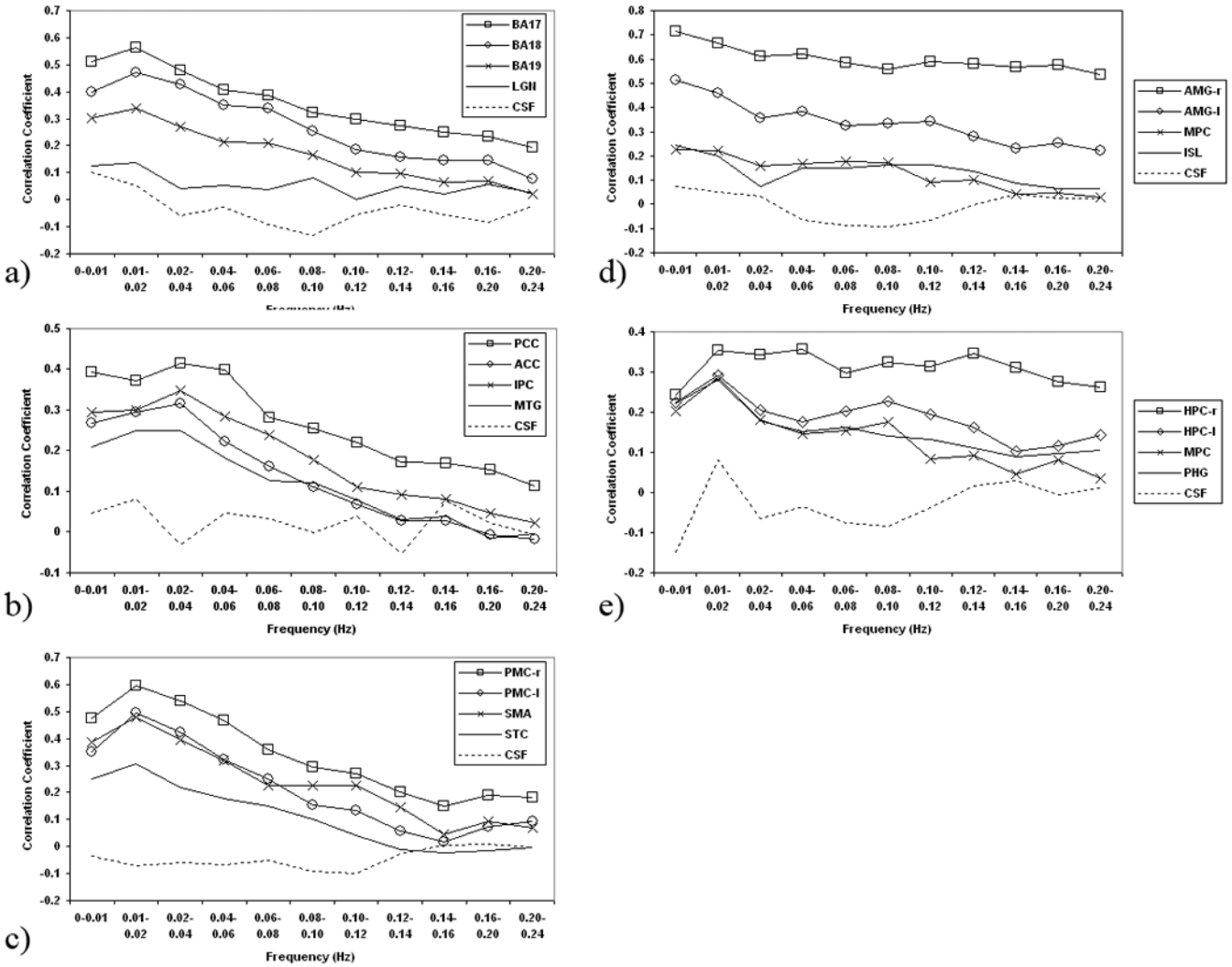

Figure 3.

Average frequency-specific connectivity strengths between the ROIs and corresponding seeds for the five brain networks—a: visual system, b: default mode, c: sensorimotor, d: amygdala, and e: hippocampus.

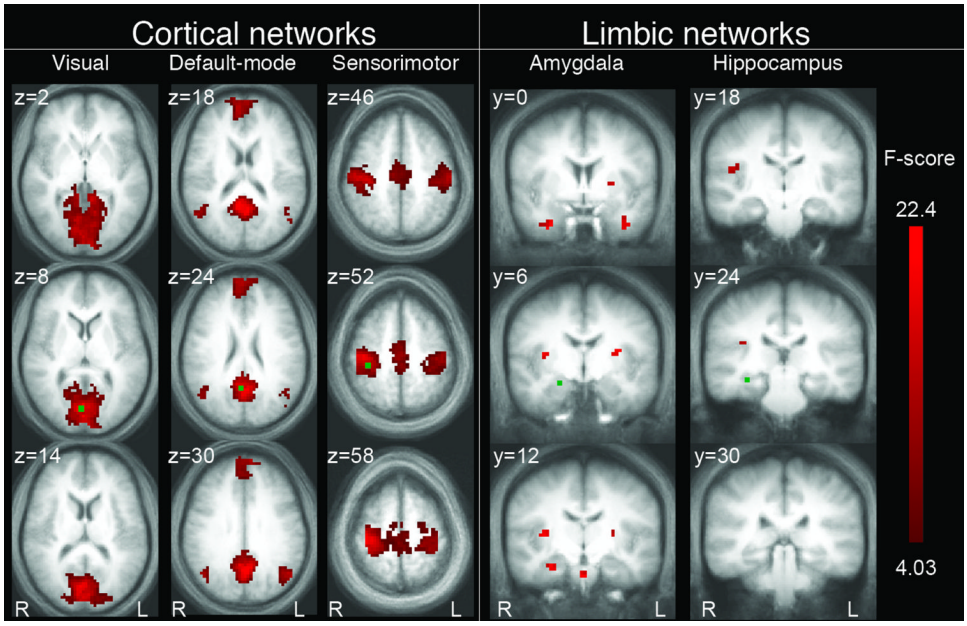

Figure 4.

F-maps ($p < 0.05$, corrected) of cortical and limbic networks, representing frequency-dependent areas within the brain networks. Each column denotes the F-maps of a network and the green dots denote the position of the seed points.

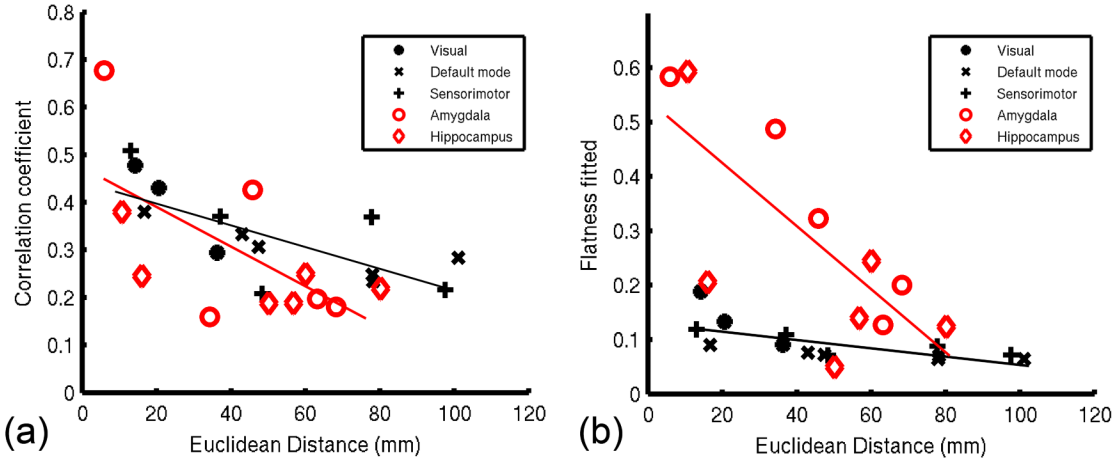

Figure 5.

(a) Correlation coefficients within the typical frequency range (0–0.1Hz) versus the Euclidean distance between ROIs to their corresponding seeds. Different distributions are observed between cortical (black) and limbic (red) networks. (b) The fitted flatness of each ROI versus the physical distance to their corresponding seed points. The salient discrepancy in Fig. 5b indicate that the resting state fMRI signal in cortical and limbic networks have distinct frequency distributions.

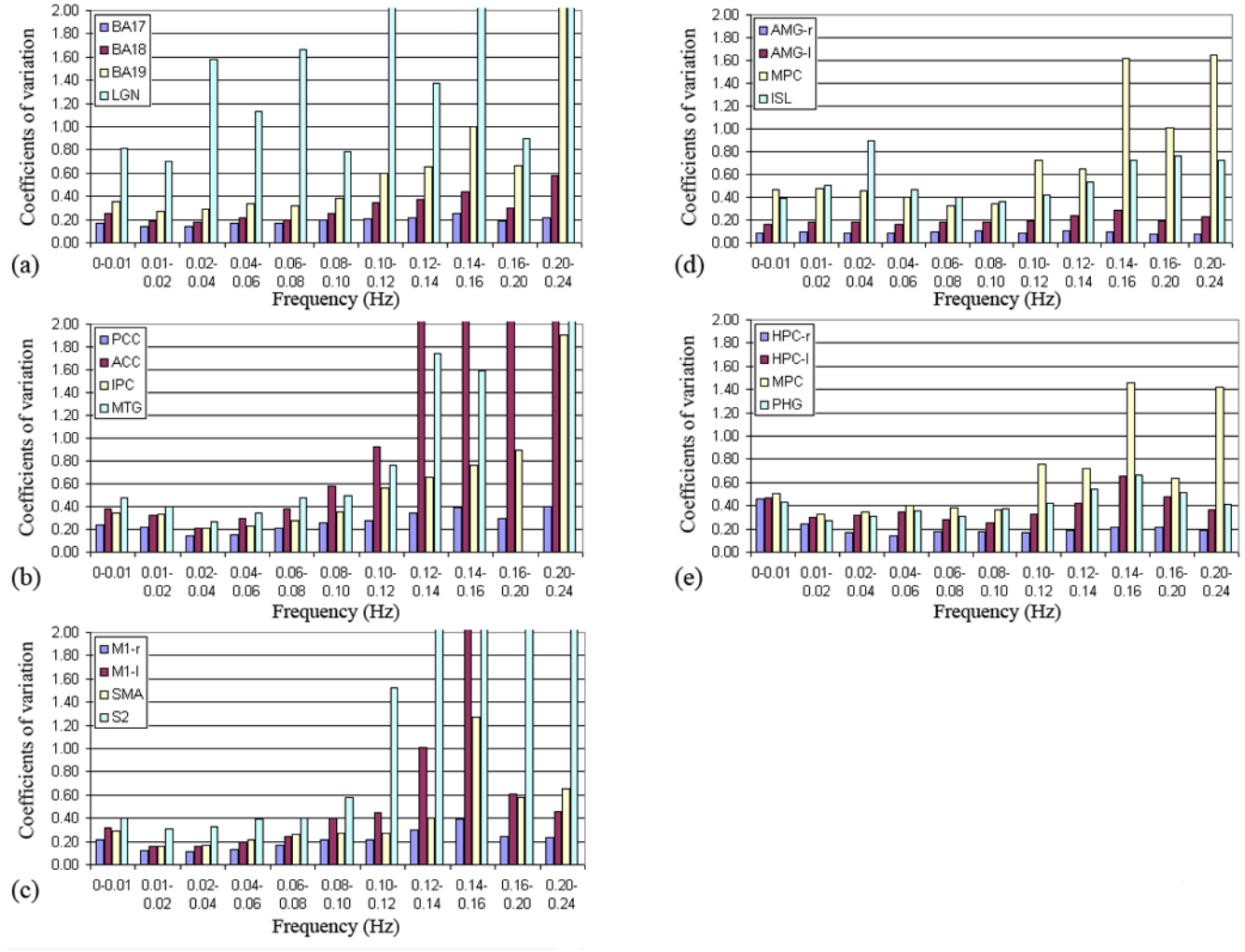

Figure 6.

Absolute coefficients of variations (CV) of ROIs from five brain networks—a: visual system, b: default mode, c: sensorimotor, d: amygdala, and e: hippocampus.

Table 1

Description of the selected seed points and ROIs for each brain network.

Network	Names of seed or region of interest	Abbr.	Talairach coordinate			Volume (mm^3)	Euclidean distance to seed (mm)
			X	Y	Z		
Visual	Primary visual area (right, seed)		3	−81	8	108	
	Primary visual area	BA17	3	−87	11	3591	14.2
	Secondary visual area	BA18	4	−79	11	13689	20.6
	Third visual area	BA19	10	−72	16	11421	36.3
	Lateral geniculate nucleus	LGN	±22	−32	3	2916	57.7
Default mode	Posterior cingulate cortex (seed)		3	−54	24	162	
	Posterior cingulate cortex	PCC	2	−57	18	12609	16.7
	Anterior cingulate cortex	ACC	3	41	32	36315	101.1
	Inferior parietal cortex (bilateral)	IPC	±43	−64	33	11826	46.1*
	Medial temporal gyrus (bilateral)	MTG	±53	−14	−9	12231	78.1*
Sensorimotor	Primary motor area (right, seed)		36	−28	53	162	
	Primary motor area (right)	M1-r	35	−28	54	12339	13
	Primary motor area (left)	M1-l	−44	−27	53	7803	77.8
	Supplementary motor area	SMA	−3	−29	59	5427	37.1
	Secondary sensory area (bilateral)	S2	±53	−23	14	22086	71.2*
Amygdala	Amygdala (right, seed)		23	−5	−15	108	
	Amygdala (right)	AMG-r	20	−8	−10	945	5.9
	Amygdala (left)	AMG-l	−25	−7	−11	1296	45.8
	Medial prefrontal cortex	MPC	−2	44	13	12717	63.2
	Insula (bilateral)	ISL	±39	−9	13	13905	51*
Hippocampus	Hippocampus (right, seed)		30	−24	−9	108	
	Hippocampus (right)	HPC-r	28	−27	−5	999	10.7
	Hippocampus (left)	HPC-l	−32	−26	−6	1161	60.1
	Medial prefrontal cortex	MPC	−2	44	13	12717	80.2
	Parahippocampal gyrus (bilateral)	PHG	±26	−34	−7	19224	36*

* the distances of bilateral ROIs were average values of left and right for facilitating the presentation.